

## Event Structure at RHIC from p-p to Au-Au

Thomas A. Trainor<sup>1</sup> (STAR Collaboration)

<sup>1</sup>CENPA 354290, University of Washington,  
Seattle, USA

**Abstract.** Several correlation analysis techniques are applied to p-p and Au-Au collisions at RHIC. Strong large-momentum-scale correlations are observed which can be related to local charge and momentum conservation during hadronization and to minijet (minimum-bias parton fragment) correlations.

*Keywords:* heavy ions, correlations, fluctuations, minijets, hadronization  
*PACS:* 25.75.Gz,24.60.Ky

### 1. Introduction

Two-particle momentum distributions from p-p and Au-Au collisions are projected onto subspaces  $(y_t \otimes y_t)$  and  $(\eta_\Delta \otimes \phi_\Delta)$  for charge-independent (CI or isoscalar) and charge-dependent (CD or isovector) charge combinations, revealing strong correlations related to parton dynamics, a color medium and changes in hadronization.

### 2. p-p Collisions: The Essential A-A Reference

The structure of hadron distributions from p-p collisions provides an essential reference for A-A collisions. Normalized  $p_t$  distributions for several event multiplicity classes of p-p collisions from RHIC at  $\sqrt{s} = 200$  GeV [1] shown in Fig. 1 (left panel) can be decomposed into a soft component and a semi-hard or minijet component. p-p event multiplicity at this energy determines the frequency of hard scatters in each event class. A two-component model function is used to describe the data:  $1/p_t dN/dp_t = n_s(n_{ch}) S_0(p_t) + n_h(n_{ch}) H_0(p_t)$ , with soft and hard reference components  $S_0(p_t)$  and  $H_0(p_t)$  (independent of  $n_{ch}$  by hypothesis) both integrating to unity on  $p_t$ . Transforming to transverse rapidity  $y_t \equiv \ln\{(m_t + p_t)/m_0\}$  as a velocity variable provides a ‘native’ description of minijets as hadron fragments from a moving source. We observe in Fig. 1 that soft-component  $S_0$  (dash-dot curve, string fragments) is well represented on transverse rapidity  $y_t$  by an error function (corresponding to a Lévy or ‘power-law’ distribution on  $m_t$ ), and hard component

$H_0$  (dashed curve, minijet fragments) is represented by a gaussian distribution on  $y_t$ , each form approximately independent of event multiplicity and determined by two parameters. The stability of the minijet fragment distribution with event multiplicity (right panel = center-panel  $- S_0(y_t)$ ) shows that gaussian distribution  $H_0$  on  $y_t$  is a good minimum-bias minijet input for A-A collision models.

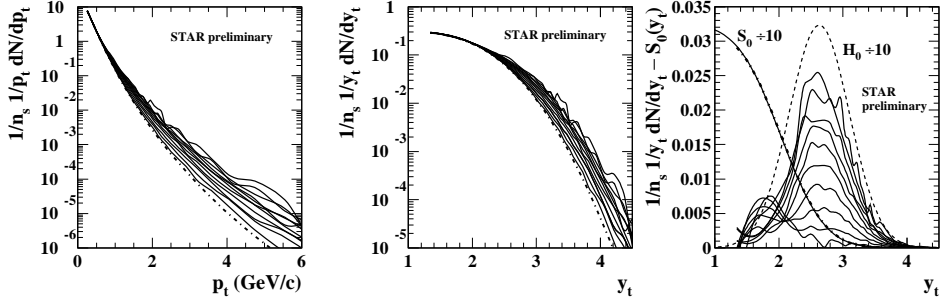


**Fig. 1.** Panels from left to right: inclusive  $p_t$  distributions for  $n_{ch} \in [1, 12]$ , same on transverse rapidity  $y_t$ , soft reference  $S_0$  subtracted to reveal hard components.

We have also measured p-p two-particle correlations [2] on transverse momentum  $p_t$  ( $0.15 \leq p_t \leq 6.0$  GeV/c) transformed to transverse rapidity  $y_t$ . We observe large-scale correlation structures also consistent with p-p collisions having soft (string) and semi-hard (minijet) components. Fig. 2 (left panel) shows correlation function  $C(y_{t1}, y_{t2}) = \rho_{sibling} - \rho_{ref}$  for STAR data. At low  $y_t$  a soft component (string fragments) falls rapidly with increasing  $y_t$ . At higher  $y_t$  the structure is centered around  $y_{t1} = y_{t2} \simeq 2.6$  ( $p_{t1} = p_{t2} \simeq 1.0$  GeV/c) and attributed to correlated fragments from semi-hard parton scatters (cf distributions in Fig. 1 (right panel)).

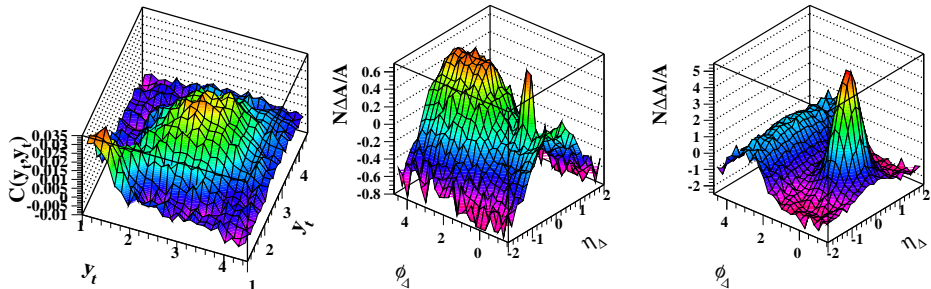


**Fig. 2.**  $y_t \otimes y_t$  correlations (left) and  $\eta_{\Delta} \otimes \phi_{\Delta}$  correlations for the soft component (center) and hard component (right) of the  $y_t \otimes y_t$  correlations.

These  $y_t \otimes y_t$  correlations provide a cut space for analysis of axial momentum correlations [2]. We construct joint autocorrelations on axial *difference variables*  $\eta_{\Delta} \equiv \eta_1 - \eta_2$  (pseudorapidity) and  $\phi_{\Delta} \equiv \phi_1 - \phi_2$  (azimuth angle) as pair-number ratio histograms. The right two panels in Fig. 2 show autocorrelations from two  $y_t$  selections in the left panel. The center panel (soft component) shows a broad peak on  $\eta_{\Delta}$  caused by local charge conservation (charge ordering) on the fragmenting string. The depression on  $\phi_{\Delta}$  near zero represents local transverse momentum conservation. The narrow peak is conversion electron pairs. The right panel (hard

component) shows a near-side peak symmetric about  $\eta_\Delta = \phi_\Delta = 0$  and a broad  $\eta_\Delta$ -independent away-side ridge. The near-side peak represents hadron fragments distributed about a common jet thrust axis, and the away-side ridge correlates particles between opposing jets. Persistence of those structures to low hadron  $p_t$  ( $\sim 0.5$  GeV) may indicate that minimum-bias partons down to  $p_t \sim 1$  GeV fragment to ‘minijets’ of one or a few hadrons.

### 3. $\langle p_t \rangle$ Fluctuations and $p_t$ Correlations in Au-Au

The scale (bin-size) dependence of event-wise mean transverse momentum  $\langle p_t \rangle$  fluctuations [ 3] can be inverted [ 4] to obtain joint  $p_t$  autocorrelations on pseudo-rapidity and azimuth angle difference variables representing velocity/temperature correlations. The structure and centrality dependence of those components suggest that the principal origin is minijets, altered by a dissipative color medium in the more central Au-Au collisions. Difference factor  $\Delta\sigma_{p_t:n}$  is related to the variance-

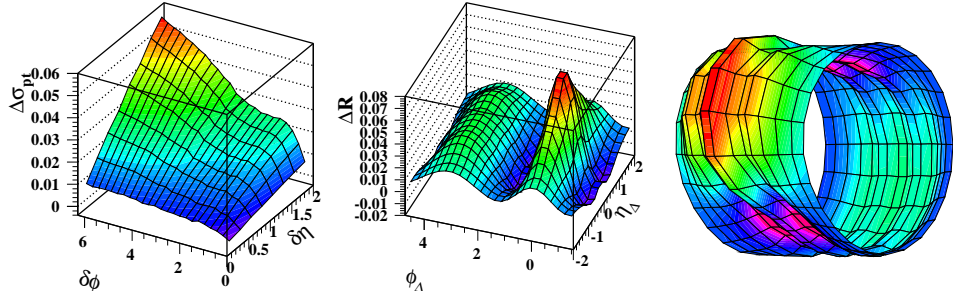


**Fig. 3.** Fluctuation scale dependence, inversion to  $p_t$  autocorrelation and same autocorrelation distribution in cylindrical format. difference measure of nonstatistical  $p_t$  fluctuations by  $\Delta\sigma_{p_t:n}^2 \equiv 2\sigma_{\hat{p}_t}\Delta\sigma_{p_t:n}$ . The variance difference is related to joint  $p_t$  autocorrelation  $\Delta R$  by integral equation

$$\Delta\sigma_{p_t:n}^2(m\epsilon_\eta, n\epsilon_\phi) \equiv 4\hat{p}_t^2 \sum_{k,l=1}^{m,n} \epsilon_\eta \epsilon_\phi K_{mn;kl} \Delta R_{kl}(p_t : n; \epsilon_\eta, \epsilon_\phi). \quad (1)$$

In Fig. 3 (left panel) is the scale variation of  $\langle p_t \rangle$  fluctuation measure  $\Delta\sigma_{p_t:n}$  for central Au-Au collisions at  $\sqrt{s_{NN}} = 200$  GeV up to the limiting STAR acceptance. The 2D joint autocorrelation on difference variables (center panel) obtained by inverting Eq. (1) has a near-side peak and away-side ridge which depend separately and strongly on collision centrality, and can be compared with Figs. 2 (right panel) and 4 (left panels). The same distribution in cylindrical format (right panel) reveals ‘necking’ on azimuth difference variable  $\phi_\Delta$ . This autocorrelation summarizes the complex velocity/temperature structure of multiple minijets in each collision averaged over many central Au-Au collisions.

#### 4. Parton Deformation in Au-Au Collisions

Charge-independent (CI) joint number autocorrelations on difference variables  $\eta_\Delta$  and  $\phi_\Delta$  were measured for particles with  $0.15 \leq p_t \leq 2 \text{ GeV}/c$  from Au-Au collisions at  $\sqrt{s_{NN}} = 130 \text{ GeV}$  [ 5]. In Fig. 4 (left panels) are autocorrelations for peripheral (d) and central (a) collisions with multipole components representing elliptic flow and momentum conservation removed, revealing minijet fragment angular distributions (conversion-electron pairs contribute to (0,0) bins). The  $(\eta, \phi)$  minijet angular correlations, symmetric about the origin in p-p and peripheral HI collisions (d), are strongly deformed in central collisions (a). Joint autocorrelations were fitted with a model function including azimuthal dipole and quadrupole terms and a 2D gaussian. Fitted gaussian widths  $\sigma_\eta$  and  $\sigma_\phi$  (right panel) *vs* centrality measure  $\nu$  (mean participant path length as number of encountered nucleons) show a dramatic centrality dependence. Minijet peak structure varies in angular shape with centrality

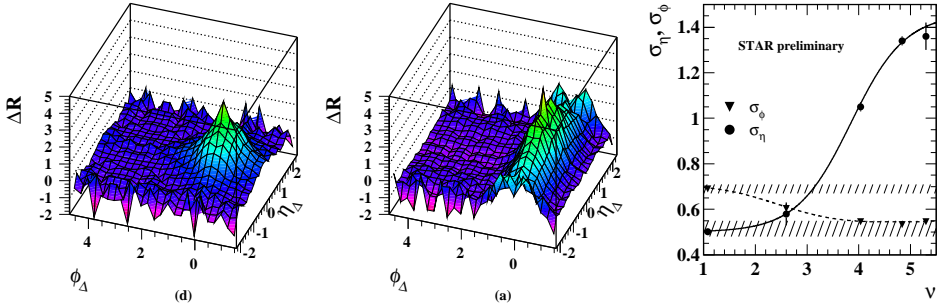


**Fig. 4.** Joint number autocorrelations with multipoles removed for peripheral (d) and central (a) events, and minijet width parameters *vs* centrality  $\nu$ . from a symmetric shape on  $(\eta_\Delta, \phi_\Delta)$  for peripheral collisions to a highly asymmetric peak for central collisions. This trend can be interpreted as a transition from *in vacuo* parton fragmentation similar to p-p collisions in peripheral heavy ion collisions to strong coupling of minimum-bias partons to a longitudinally-expanding color medium in central collisions. This result is inconsistent with pQCD-based models of jet quenching but may favor some recombination models.

#### 5. Centrality Evolution of Hadronization Geometry

Charge-dependent (CD) joint number autocorrelations on difference variables  $\eta_\Delta$  and  $\phi_\Delta$  were measured for primary charged hadrons with  $0.15 \leq p_t \leq 2 \text{ GeV}/c$  from Au-Au collisions at  $\sqrt{s_{NN}} = 130 \text{ GeV}$  [ 5]. Large-scale correlation structures, not predicted by theory, are consistent with a change in the geometry of hadron emission with increasing centrality of Au-Au collisions. In p-p collisions charge-dependent correlations are dominated by a 1D gaussian on  $\eta_\Delta$  indicative of charge-ordering on the axial string as shown with the Pythia Monte Carlo in Fig. 5 (left panel). In central Au-Au collisions CD correlations are dominated by a peak at  $(0,0)$  nearly exponential in shape and nearly symmetric on  $(\eta, \phi)$ . Fig. 5

(center panel) shows CD correlations for the most peripheral event class (d) in this study, in which the central 2D exponential peak and the 1D gaussian peak on  $\eta_\Delta$  coexist. Joint autocorrelations for four centrality classes were fitted with a model consisting of a 2D exponential with independent widths on  $\eta_\Delta$  and  $\phi_\Delta$ , and a 1D gaussian on  $\eta_\Delta$ . Fitted width parameters are shown (right panel) *vs* centrality measure  $\nu$ . These data are consistent with local charge conservation or

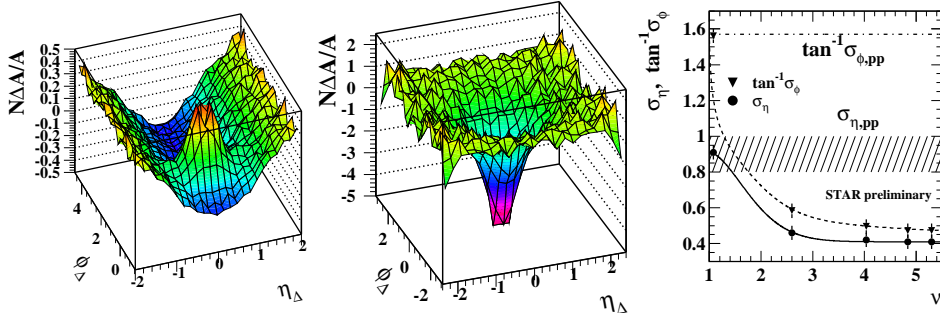


**Fig. 5.** Charge-dependent number autocorrelations for p-p collisions, central Au-Au collisions, and width parameters *vs* centrality measure  $\nu$ .

canonical suppression of net charge fluctuations. The strong variation of correlation structure from p-p to peripheral Au-Au to central Au-Au can be interpreted as follows: Hadronization geometry evolves from 1D color-string fragmentation in p-p collisions to exponentially-attenuated 2D charge-ordered emission from a hadron-opaque medium in central Au-Au collisions. These results are qualitatively inconsistent with standard HI collision models and predictions of QGP-related strong suppression of net-charge fluctuations.

## 6. Energy Dependence of $\langle p_t \rangle$ Fluctuations

Controversy has emerged over the  $\sqrt{s_{NN}}$  dependence of  $\langle p_t \rangle$  fluctuations in heavy ion collisions from SPS to RHIC energies. Analysis of  $p_t$  autocorrelations (*cf* Sec. 3) at 20 and 200 GeV indicates a strong and monotonic increase with collision energy, with nontrivial  $\langle p_t \rangle$  fluctuations first appearing at a threshold of observability near 10 GeV. Analysis based on ‘temperature’ fluctuations on the other hand [ 6] suggests that  $\langle p_t \rangle$  fluctuations are nearly independent of collision energy over this interval. In Fig. 6 (left two panels) is a comparison of *per particle*  $p_t$  autocorrelations inferred from STAR  $\langle p_t \rangle$  fluctuation scale dependence at 20 and 200 GeV [ 3], with the same detector and analysis system in each case. There is evident a dramatic difference in fluctuations/correlations between SPS ( $\sim$  20 GeV) and RHIC ( $\sim$  200 GeV) energies. The right-most panel shows the trend on collision energy of the large-scale correlation (LSC) component of  $p_t$  autocorrelations at five cm energies (12.6, 17.8, 20, 130 and 200 GeV) projected onto difference variable  $\eta_\Delta$ . This projection permits direct comparison with CERES’ measurements of  $\Phi_{p_t}(\delta\eta) \approx \Delta\sigma_{p_t:n}(\delta\eta)$  variation with pseudorapidity bin size [ 6]. LSC, defined as the autocorrelation amplitude

at *large*  $\eta_\Delta$ , is distinguished from small-scale correlations (SSC), which especially at SPS energies are dominated by HBT (quantum) and Coulomb correlations. We observe that the principal mechanism for  $\langle p_t \rangle$  fluctuations at RHIC is minijets. The energy dependence of the LSC component is therefore of considerable interest: what is the energy trend of semi-hard parton scattering, as manifested by correlated hadron fragments, down to the lowest relevant energy?

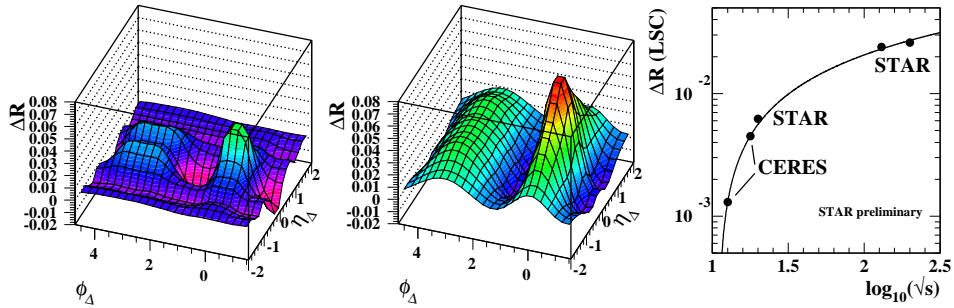


**Fig. 6.** STAR  $p_t$  autocorrelations at 20 and 200 GeV, and energy dependence of large-scale correlations (LSC) from SPS to RHIC energies.

## 7. Conclusions

By comparing correlation structures in p-p and Au-Au collisions obtained by several analysis methods we have gained important new information about the changing geometry of hadronization and about the interaction of low- $p_t$  partons with a color medium generated in the more central Au-Au collisions.

## References

1. T. A. Trainor (STAR Collaboration), Bull. Am. Phys. Soc. **48**, 25 (2003).
2. R. J. Porter (STAR Collaboration), Bull. Am. Phys. Soc. **48**, 25 (2003).
3. T. A. Trainor (STAR Collaboration), Bull. Am. Phys. Soc. **48**, 25 (2003).
4. D. J. Prindle (STAR Collaboration), Bull. Am. Phys. Soc. **48**, 25 (2003).
5. A. Ishihara (STAR Collaboration), Bull. Am. Phys. Soc. **48**, 25 (2003).
6. D. Adamova *et al.* (CERES Collaboration), Nucl. Phys. A **727**, 97 (2003).